1 Supplementary material for LHCb-PAPER-2020-047

This appendix contains supplementary material that will be posted on the public CDS record but will not appear in the paper.

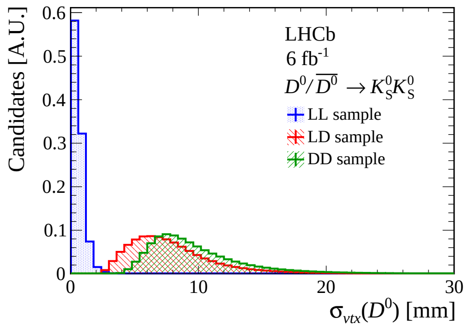

Figure 1: D^0 decay vertex uncertainty distribution for $D^0 \to K_S^0 K_S^0$ decays. The distributions are plotted in blue for the LL sample, in red for the LD sample and in green for the DD sample.

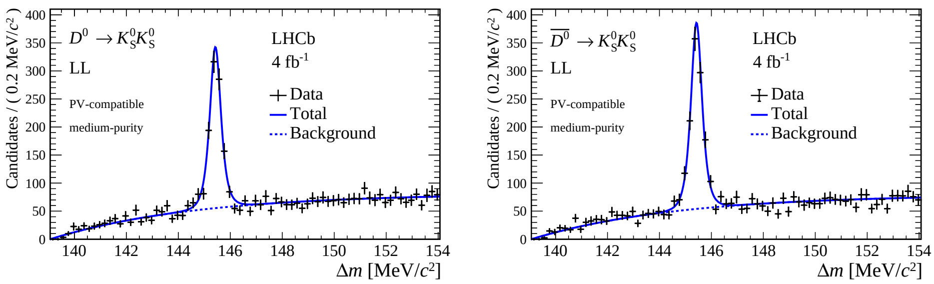

Figure 2: Distributions and fit projections of Δm for D^0 (left) and $\overline{D}^0$ (right) decays for the 2017–2018 PV-compatible LL sample.

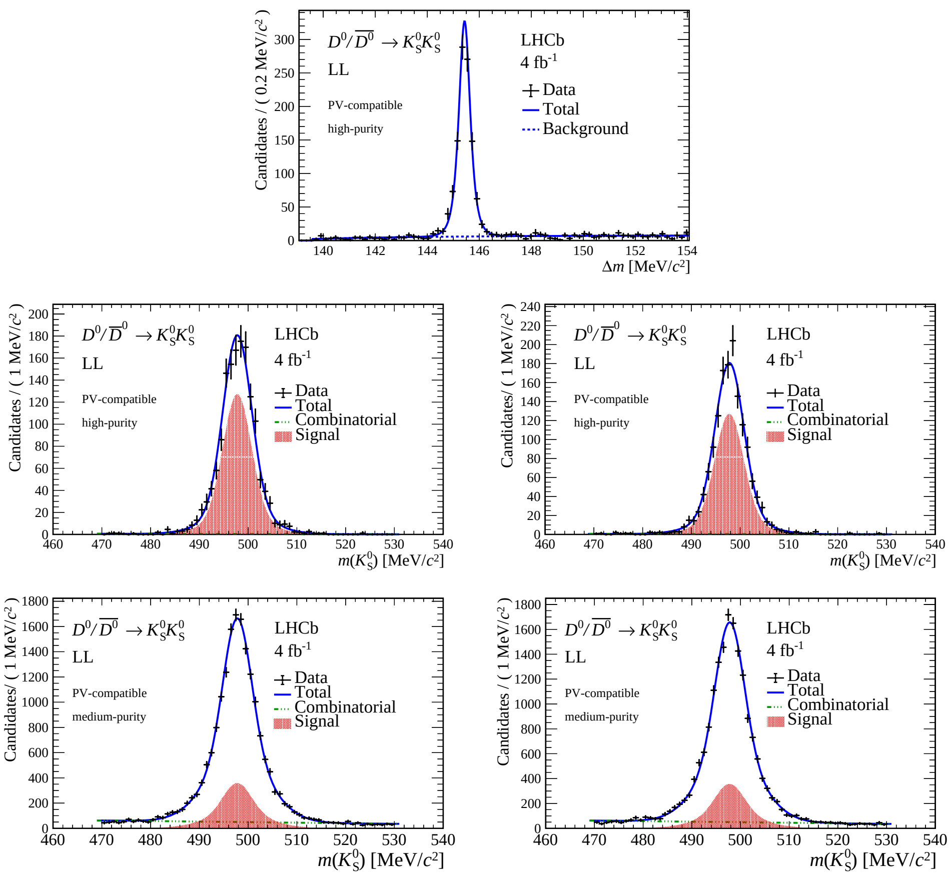

Figure 3: Charge-integrated mass distributions and fit projections for LL PV-compatible sample (2017–2018 data). Top: Δm distribution. Middle and bottom: $m(K^0_S)$ distributions for the two K^0_S candidates (left, right) in the two ranges of classifier output. The mass range for L K^0_S candidates is limited to [470,530] MeV/c^2 by a trigger requirement.

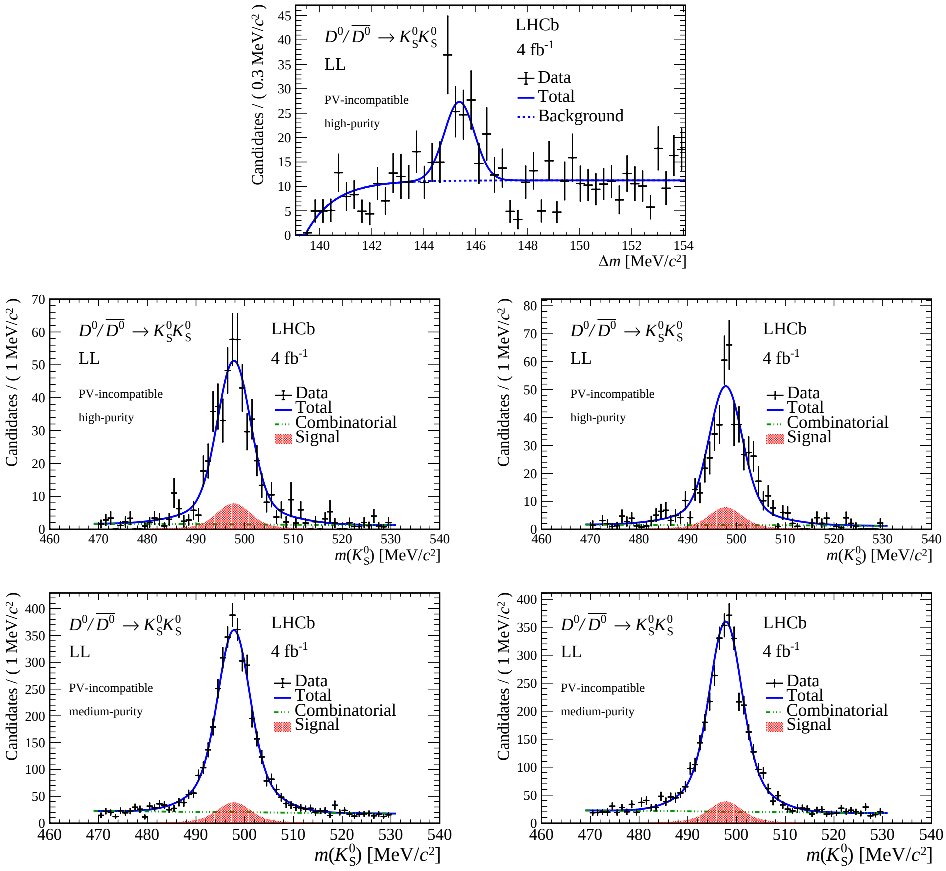

Figure 4: Charge-integrated mass distributions and fit projections for LL PV-incompatible sample (2017–2018 data). Top: Δm distribution. Middle and bottom: $m(K^0_S)$ distributions for the two K^0_S candidates (left, right) in the two ranges of classifier output. The mass range for L K^0_S candidates is limited to [470,530] MeV/c^2 by a trigger requirement.

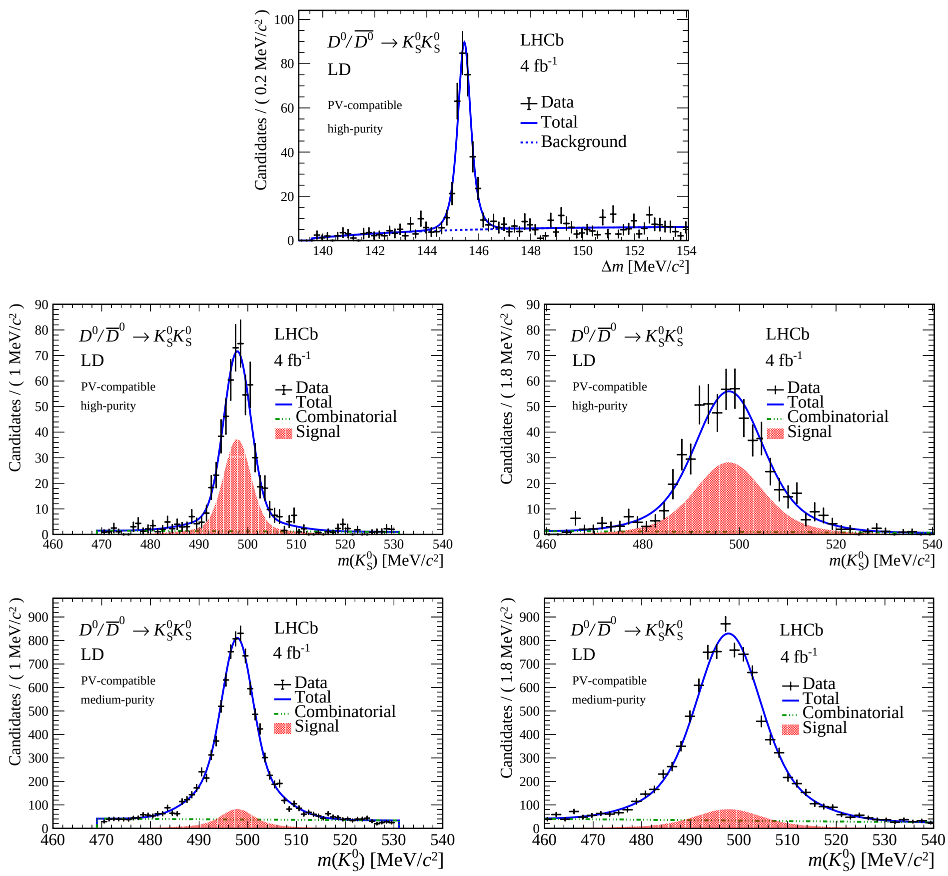

Figure 5: Charge-integrated mass distributions and fit projections for LD PV-compatible sample (2017–2018 data). Top: Δm distribution. Middle and bottom: $m(K^0_S)$ distributions for L (left) and D (right) K^0_S candidates in the two ranges of classifier output. The mass range for L K^0_S candidates is limited to [470,530] MeV/c^2 by a trigger requirement.

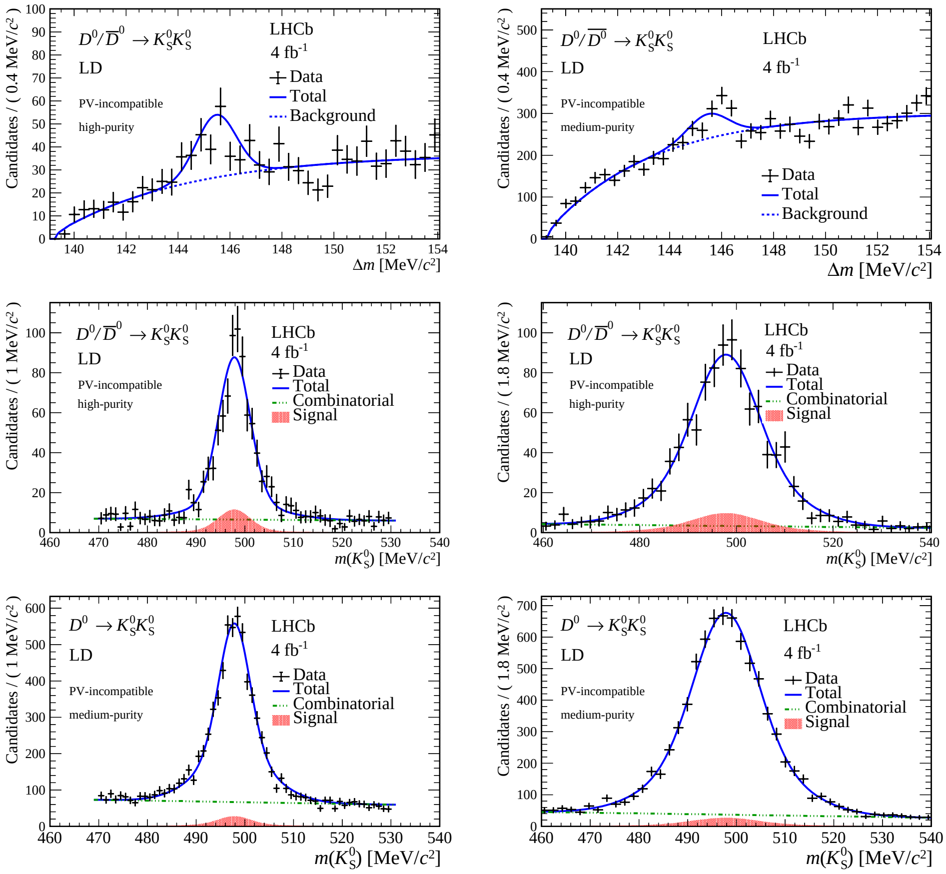

Figure 6: Charge-integrated mass distributions and fit projections for LD PV-incompatible sample (2017–2018 data). Top: Δm distribution for the two ranges of classifier output. Middle and bottom: $m(K_S^0)$ distributions for L (left) and D (right) K_S^0 candidates in the two ranges of classifier output. The mass range for L K_S^0 candidates is limited to [470,530] MeV/c^2 by a trigger requirement.

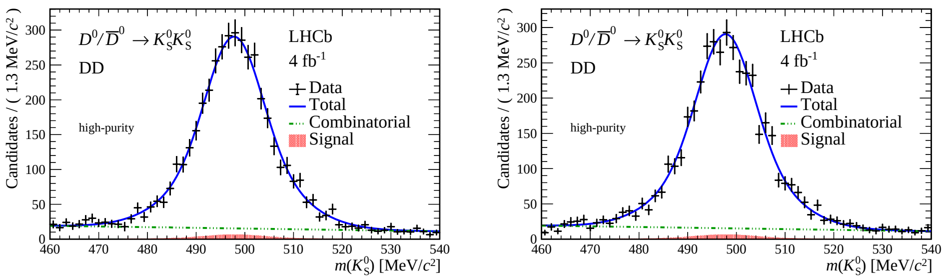

Figure 7: Charge-integrated mass distributions for the two K_S^0 in the DD sample (2017–2018 data).

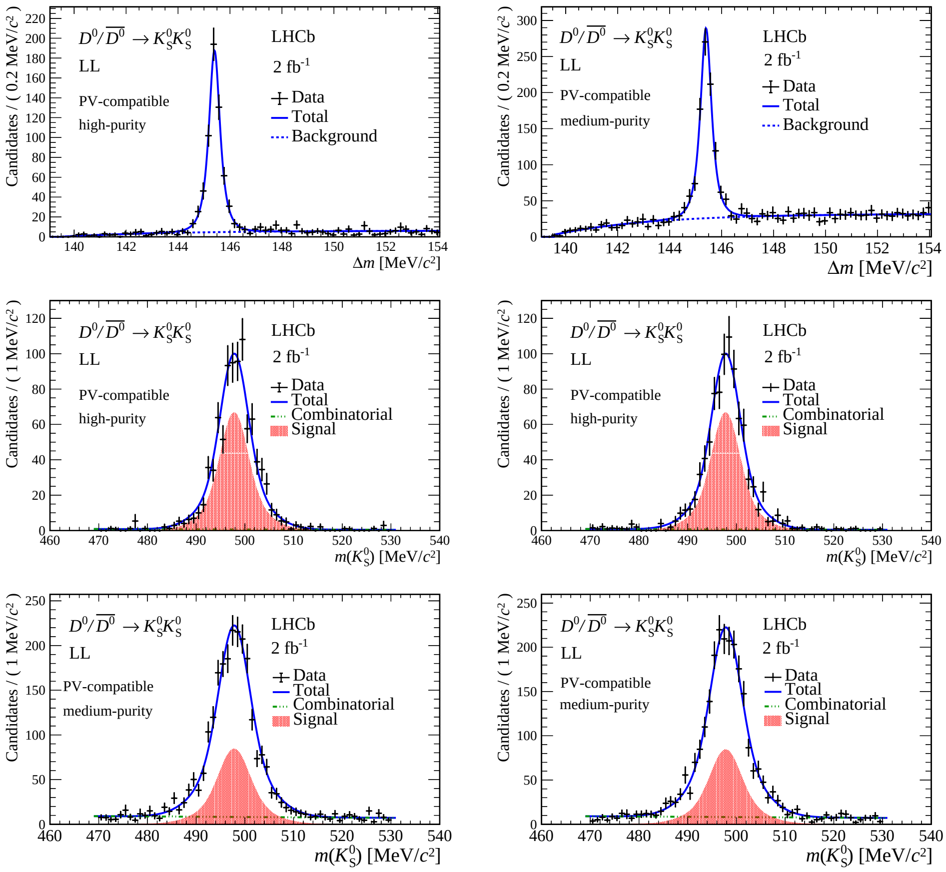

Figure 8: Charge-integrated mass distributions and fit projections for LL PV-compatible sample (2015–2016 data). Top: Δm distributions for the two ranges of classifier output. Middle and bottom: $m(K^0_S)$ distributions for the two K^0_S candidates (left, right) in the two ranges of classifier output. The mass range for L K^0_S candidates is limited to [470,530] MeV/c^2 by a trigger requirement.

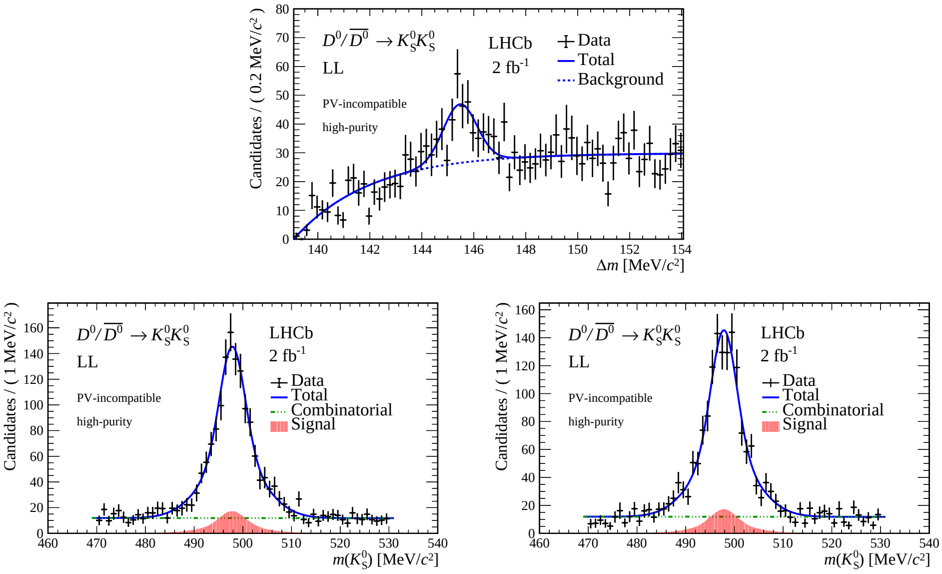

Figure 9: Charge-integrated mass distributions and fit projections for LL PV-incompatible sample (2015–2016 data). Top: Δm distribution. Bottom: $m(K^0_S)$ distributions for the two K^0_S candidates. The mass range for L K^0_S candidates is limited to $[470{,}530]\,\text{MeV}/c^2$ by a trigger requirement.

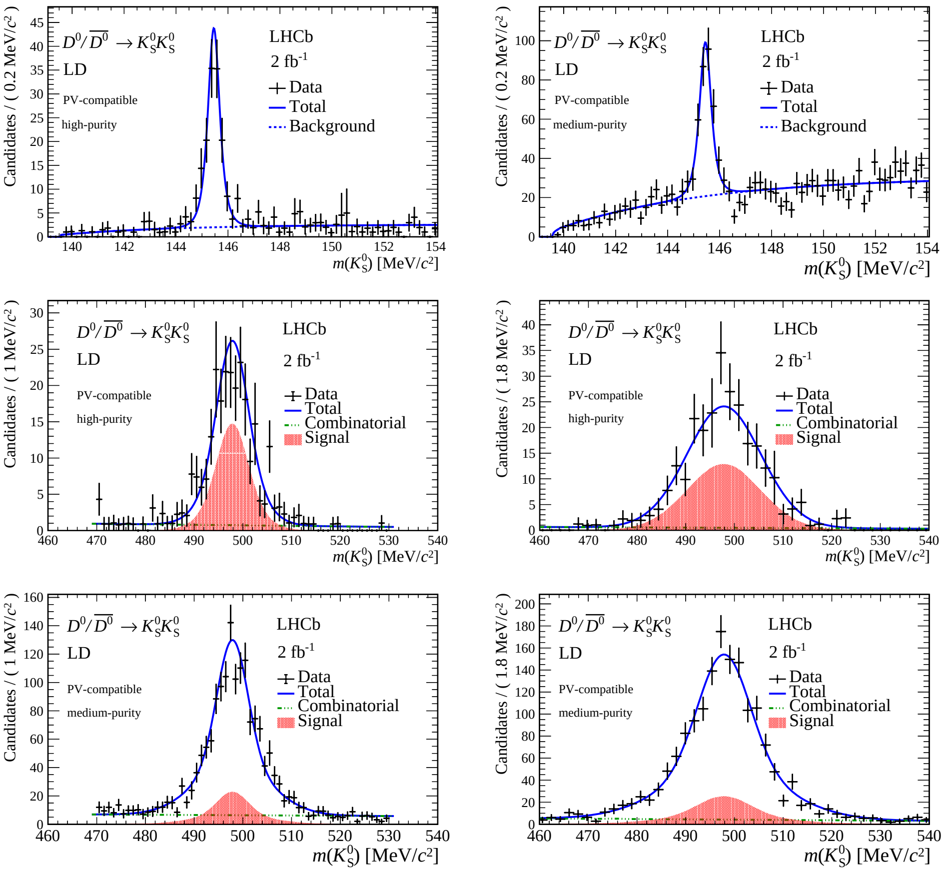

Figure 10: Charge-integrated mass distributions and fit projections for LD PV-compatible sample (2015–2016 data). Top: Δm distributions for the two ranges of classifier output. Middle and bottom: $m(K_S^0)$ distributions for L (left) and D (right) K_S^0 candidates in the two ranges of classifier output. The mass range for L K_S^0 candidates is limited to [470,530] MeV/c^2 by a trigger requirement.

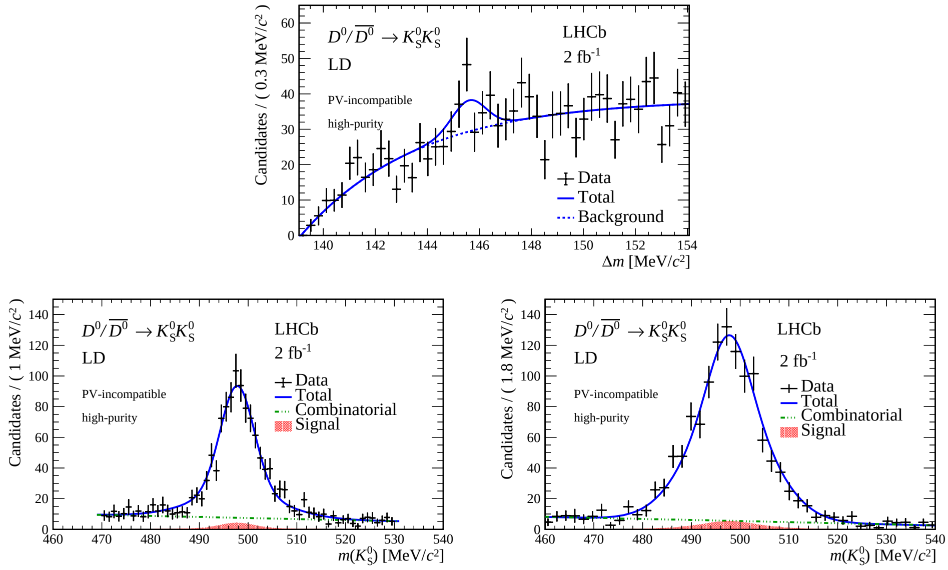

Figure 11: Charge-integrated mass distributions and fit projections for LD PV-incompatible sample (2015–2016 data). Top: Δm distribution. Bottom: $m(K^0_S)$ distributions for L (left) and D (right) K^0_S candidates. The mass range for L K^0_S candidates is limited to [470,530] MeV/c^2 by a trigger requirement.

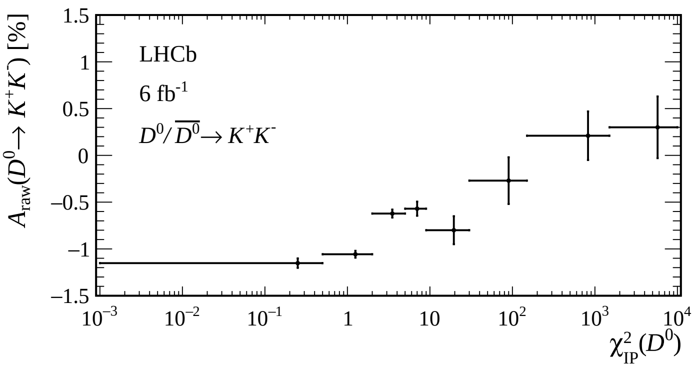

Figure 12: Raw asymmetry, evaluated on the $D^0 \to K^+K^-$ calibration sample, as a function of $\chi^2_{\rm IP}(D^0)$.

Here a step-by-step derivation of Eq. (3) is given. Start by noting that weighting events with the weight defined by Eq. (3), in the limit of large numbers, leads to a total number of events given by:

$$N_W^{\pm} = \int \frac{1 \pm \mathcal{A}^{CP}(K^+K^-)}{2n_C^{\pm}(\vec{p}_0)}[n_C^+(\vec{p}_0) + n_C^-(\vec{p}_0)]n_S^{\pm}(\vec{p}_0)d\vec{p}_0 \tag{1}$$

This is effectively a Monte Carlo approximation to the above integral.

The integrand in Eq. (1) can be rewritten as:

$$\frac{[1 \pm \mathcal{A}^{CP}(K^+K^-)][n_C^+(\vec{p}_0) + n_C^-(\vec{p}_0)]}{2N \int \epsilon_C^{\pm}(\vec{p}_0, \vec{p}_*)p_C^{\pm}(\vec{p}_0, \vec{p}_*)d\vec{p}_*}n_S^{\pm}(\vec{p}_0), \tag{2}$$

where N is the number of pp collisions, $\epsilon_C^{\pm}(\vec{p}_0, \vec{p}_*)$ is the overall efficiency for detecting a $D^{*\pm}$ in the calibration channel, and $p_C^{\pm}(\vec{p}_0, \vec{p}_*)$ is the probability density for producing a $D^{*\pm} \to D^0\pi^{\pm}$ decay, where the $D^{*\pm}$ and the D^0 have respectively momentum $\vec{p}_*$ and $\vec{p}_0$ and the given charge, with the subsequent $D^0 \to K^+K^-$ decay (the "C" suffix stands for "calibration").

It can be noted that $\epsilon_C^{\pm}(\vec{p}_0, \vec{p}_*) = \epsilon^{\pm}(\vec{p}_*)\epsilon_C(\vec{p}_0)$, where $\epsilon_C(\vec{p}_0)$ is the efficiency for detecting a D^0 decaying into the calibration channel and $\epsilon^{\pm}(\vec{p}_*)$ is the (relative) efficiency for detecting a $D^{*\pm}$. The latter is assumed to be independent of D^0 kinematics and decay mode (D^0 final states are charge-symmetric), but is allowed to have arbitrary dependency on $\vec{p}_*$, and be different for each charge.

In addition, the following equality holds:

$$p_C^{\pm}(\vec{p}_0, \vec{p}_*) = p_{\pm}(\vec{p}_*)p_0(\vec{p}_0|\vec{p}_*)B_C(1 \pm \mathcal{A}^{CP}(K^+K^-))/2,$$

where $p_{\pm}(\vec{p}_*)$ is the probability density for producing a $D^{*\pm}$ of momentum $\vec{p}_*$ in a single pp collision, $p_0(\vec{p}_0|\vec{p}_*)$ is the probability density for producing a D^0 or $\overline{D}^0$ candidate with a momentum $\vec{p}_0$, conditional on $\vec{p}_*$, and B_C is the branching ratio. Therefore, the quantity in Eq. (2) can be rewritten as

$$\frac{[1 \pm \mathcal{A}^{CP}(K^+K^-)][n_C^+(\vec{p}_0) + n_C^-(\vec{p}_0)]}{2N \int \epsilon_C^{\pm}(\vec{p}_0, \vec{p}_*)p_{\pm}(\vec{p}_*)p_0(\vec{p}_0|\vec{p}_*)B_C/2(1 \pm \mathcal{A}^{CP}(K^+K^-))d\vec{p}_*}n_S^{\pm}(\vec{p}_0) =$$

$$= \frac{2n_S^{\pm}(\vec{p}_0)[n_C^+(\vec{p}_0) + n_C^-(\vec{p}_0)]}{2N \int \epsilon_C^{\pm}(\vec{p}_0, \vec{p}_*)p_{\pm}(\vec{p}_*)p_0(\vec{p}_0|\vec{p}_*)B_C d\vec{p}_*} =$$

$$= \frac{2[n_C^+(\vec{p}_0) + n_C^-(\vec{p}_0)] \int \epsilon_S^{\pm}(\vec{p}_0, \vec{p}_*)p_S^{\pm}(\vec{p}_0, \vec{p}\vec{p}_*}{2B_C \int \epsilon_C^{\pm}(\vec{p}_0, \vec{p}_*)p_{\pm}(\vec{p}_*)p_0(\vec{p}_0|\vec{p}_*)d\vec{p}_*}$$

$$= \frac{[n_C^+(\vec{p}_0) + n_C^-(\vec{p}_0)]\epsilon_S(\vec{p}_0) \int \epsilon^{\pm}(\vec{p}_*)p_{\pm}(\vec{p}_*)p_0(\vec{p}_0|\vec{p}_*)B_S(1 \pm \mathcal{A}^{CP}(K_S^0K_S^0))d\vec{p}_*}{2B_C\epsilon_C(\vec{p}_0) \int \epsilon^{\pm}(\vec{p}_*)p_{\pm}(\vec{p}_*)p_0(\vec{p}_0|\vec{p}_*)d\vec{p}_*},$$

where the "S" suffix labels the quantities already defined above, but for the "signal" $D^0 \to K_S^0K_S^0$ sample. This can be further rewritten as

$$\frac{[n_C^+(\vec{p}_0) + n_C^-(\vec{p}_0)]\epsilon_S(\vec{p}_0)B_S(1 \pm \mathcal{A}^{CP}(S))}{2B_C\epsilon_C(\vec{p}_0)} \times \frac{\int \epsilon^{\pm}(\vec{p}_*)p_{\pm}(\vec{p}_*)p_0(\vec{p}_0|\vec{p}_*)d\vec{p}_*}{\int \epsilon^{\pm}(\vec{p}_*)p_{\pm}(\vec{p}_*)p_0(\vec{p}_0|\vec{p}_*)d\vec{p}_*} =$$

$$= \frac{B_S \epsilon_S(\vec{p}_0)}{2B_C \epsilon_C(\vec{p}_0)} (1 \pm \mathcal{A}^{CP}(K^0_S K^0_S))(n^+_C(\vec{p}_0) + n^-_C(\vec{p}_0))$$

and therefore

$$N^{\pm}_W = \frac{B_S}{2B_C}(1 \pm \mathcal{A}^{CP}(K^0_S K^0_S)) \int \frac{\epsilon_S(\vec{p}_0)}{\epsilon_C(\vec{p}_0)}(n^+_C(\vec{p}_0) + n^-_C(\vec{p}_0)) d\vec{p}_0$$

Note that the above integral is now charge-independent, so it drops out in the event number asymmetry:

$$\mathcal{A}^{CP}(K^0_S K^0_S) = \frac{N^+_W - N^-_W}{N^+_W + N^-_W}, \quad (3)$$

leading to an unbiased estimate of the *CP* asymmetry of the channel of interest.